BER Analysis of a NOMA Enhanced Backscatter Communication System

Ahsan Waleed Nazar*, Syed Ali Hassan†, Haejoon Jung‡
School of Electrical Engineering & Computer Science (SEECS),
National University of Sciences & Technology (NUST) Pakistan
Email: *anazar.msee23mcs@students.mcs.edu.pk, †ali.hassan@seecs.edu.pk
‡Dept. of Information and Telecommunication Engineering,
Incheon National University, Korea
Email: ‡haejoonjung@inu.ac.kr

GLOBECOM 2020 - 2020 IEEE Global Communications Conference | 978-1-7281-8298-8/20/$31.00 ©2020 IEEE | DOI: 10.1109/GLOBECOM42002.2020.9322119

***Abstract*—Backscatter communication (BackCom) has been emerging as a prospective candidate in tackling lifetime management problems for massively deployed Internet-of-Things (IoT) devices. This passive sensing approach allows a backscatter node (BN) to transmit information by reflecting the incident signal from a reader without initiating its transmission. Power-domain non-orthogonal multiple access (PD-NOMA), i.e., multiplexing the BNs with different backscatter power levels, being a prime candidate for multiple access in 5G systems is fully exploited in this work to multiplex multiple BNs. Recently, a great deal of attention has been devoted to the study of NOMA-aided BackCom networks in the context of outage probabilities and system throughput. However, the exact closed-form expressions of bit error rate (BER) for such a system has not been studied in the literature. In this paper, we derive the analytical BER expressions for a two BN BackCom system employing NOMA with imperfect successive interference cancellation (SIC) over an additive white Gaussian noise (AWGN) channel. The obtained BER expressions are utilized to evaluate the optimum reflection coefficients of BNs needed for the most optimal system performance in terms of BER and range of communication.**

***Index Terms*—Backscatter communication (BackCom), non-orthogonal multiple access (NOMA), Internet-of-things (IoT), bit error rate (BER).**

I. Introduction

The Internet-of-things (IoT) proliferation in the context of massive machine type communication (mMTC) is one of the key technology trends driving the fifth-generation (5G) networks innovation [1]. IoT cellular devices connectivity is expected to reach 5.0 billion devices by 2025 because of its immense applicability in the smart home, smart city, smart agriculture, connected health, smart industries, autonomous vehicles, and unmanned aerial vehicles (UAVs) [2]. For instance, in smart cities, an IoT network can provide efficient waste management, parking assistance, and air quality monitoring. Similarly, in smart agriculture, such an IoT network can be used to monitor soil moisture, pest control mechanisms, and livestock tracking [3], [4].

With such a huge deployment of IoT sensors, the lifetime management of devices becomes critical, and conventional battery-based solutions are not viable due to the high cost of battery replacements and recycling concerns. Furthermore, battery recharging is especially challenging when most of the sensors are hidden (e.g., inside walls) or deployed in an inaccessible environment (e.g., under cultivated land). Recently, energy harvesting solutions are proposed to overcome the aforementioned problems in IoT devices [5]. For such massive IoT networks, backscatter communication (BackCom) is one of the promising energy harvesting techniques [6]. A BackCom system is generally composed of two components, a backscatter reader and backscatter nodes (BNs). The BN is not equipped with an active radio frequency (RF) transmission component for information transfer rather it relies on the unmodulated carrier signal transmitted by the reader for both energy harvesting and backscatter.

This backscatter is made possible because of the intentional impedance mismatch at the antenna input which results in different reflection coefficients [7]. Data encoding for backscatter over an incident wave is carried out by varying the reflection coefficients at the antenna input side. This backscatter approach is vastly different from the generally applied wireless harvesting approach where nodes first harvest energy to perform active RF transmission. Therefore, transmissions in a backscatter communication consume orders of magnitude less energy than a typical radio and the absence of an active RF component in BNs results in simpler and low complexity circuits. Therefore, BackCom approach is most suitable for IoT communications [8].

The BackCom system, consisting of multiple BNs that reflect the incident CW signal originating from a single reader, needs an efficient multiple access mechanism to accommodate the maximum number of BNs without sacrificing spectral efficiency and user fairness. Non-orthogonal multiple access (NOMA) is the prime candidate to handle multiple access in such a one-to-many BackCom uplink communication system [9], [10]. Power domain NOMA exploits the channel differences among users for multiplexing and is envisaged as an essential technology for 5G systems because of its low latency and high spectral efficiency [11], [12]. In [13], the authors investigated the performance of a NOMA-enhanced BackCom system, and the significance of adopting NOMA with the BackCom system was demonstrated by analyzing the average number of successfully decoded bits. Similarly, authors in [14] evaluated the performance of NOMA-aided BackCom

978-1-7281-8298-8/20/$31.00 ©2020 IEEE

network in terms of outage probability and system throughput. The authors in [15] and [16] study the problem of resource allocation in NOMA-enhanced backscatter communication network. In [17], the authors analyzed the outage probabilities and the ergodic rate for a novel symbiotic system which integrates NOMA and ambient BackCom.

In this work, we consider a NOMA-enhanced backscatter uplink communication where one reader serves a cluster of two randomly deployed BNs. The reflection coefficients of the BNs are set different from each other to make the wireless channel distinct to better exploit power-domain NOMA. The proposed scheme results in increased spectrum efficiency and reduced collisions among the BNs. The main contributions of this paper are summarized as follows:

- The BER performance of a NOMA enhanced BackCom system with imperfect SIC is considered, where exact closed-form analytical BER expressions of binary phase-shift keying (BPSK) are derived for two BNs. The derived BER expressions are verified by Monte Carlo simulations for various reflection coefficients.
- The increase in effective non-erroneous transmitted bits over a large period in a NOMA-BackCom scheme is compared with an OMA scheme for optimal and non-optimal reflection coefficient conditions. Moreover, the significance of setting the right reflection coefficients is also illustrated.
- Based on the derived analytical equations, the analysis of optimal reflection coefficients for two BNs is carried out and the theoretical BNs coverage range for acceptable BER behavior has been found for several reflection coefficients.

The rest of the paper is organized as follows. In Sec. II, the system model of the NOMA-aided BackCom system is briefly described. It is followed by the explicit closed-form BER expressions of BPSK constellation for two BNs in Sec. III. Numerical and simulation results are shown in Sec. IV. Finally, conclusions are presented in Sec. V.

II. System Model

In this paper, we consider the case of a single backscatter reader and a single cluster consisting of two semi-passive BNs. The BNs do not effectively transmit any radio signal, instead, the reader sends a continuous wave (CW) signal to the BNs. After energy harvesting to support the operations of sensing and micro-controller, the BNs reflect the incident CW signal to achieve communication with the reader. This backscatter is carried out by modulating the incoming signal using variable impedance. Due to the energy and complexity constraints of a BackCom system, BPSK modulation is considered in this work, where the modulation is performed by changing the load impedance between two impedance states through a micro-controller. These two impedance states correspond to the same magnitude but with two different phase shifts.

An uplink NOMA scheme is utilized in this system, whereby, both BNs reflect the incoming signal by sharing the same time-frequency resource. The received signal at the reader undergoes double attenuation effects due to dyadic channel from reader to the BNs and back. Fig. 1 illustrates the corresponding schematic of the uplink NOMA scheme. The received signal at the reader is given by

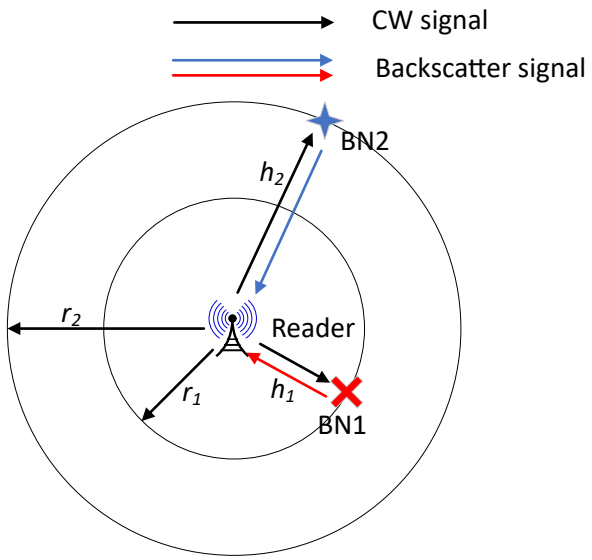

Fig. 1. Illustration of uplink NOMA-BackCom system

$$y = \sqrt{P_r \xi_1} h_1 x_1 + \sqrt{P_r \xi_2} h_2 x_2 + w, \tag{1}$$

where ξ_i $(i \in \{1, 2\})$ and h_i denote the power reflection coefficient of BNs and channel coefficients between the BNs and the reader. Because of the small coverage region of a BackCom system, a strong line-of-sight (LOS) link is assumed between the reader and the BNs and, therefore, a path loss-only channel model is considered which consists of the double attenuation effect (i.e., $r_i^{2\alpha}$, where r_i denote the distance between the reader and the i-th BN and α is the path loss exponent). In (1), P_r is the reader transmit power, x_i is the BPSK modulated information signal of user i, and w is additive white Gaussian noise (AWGN) with zero mean and N_0 variance.

A successive interference cancellation (SIC) process is implemented at the reader to decode the two users' signals. For uplink NOMA, the optimal order of decoding is in the order of decreasing channel gains and it is assumed in our study that $|h_1|^2 > |h_2|^2$. Because of stronger channel conditions, the signal from user 1, u_1, is decoded first by treating user 2, u_2, as inter-user interference (IUI) at the reader. Next, u_2 signal is decoded after subtracting the detected u_1 symbol from received composite signal y. If u_1's signal is decoded correctly then no IUI is faced in decoding of u_2, otherwise, there will be error propagation from u_1 when decoding u_2. In conventional power-domain NOMA, the multiplexed devices can transmit with different powers to accrue maximum benefit from NOMA. However, in a BackCom system, owing to no active RF transmission capability, the BNs reflect with

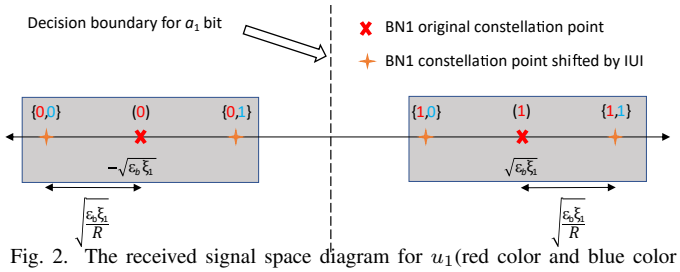

Fig. 2. The received signal space diagram for u_1(red color and blue color represent u_1 and u_2 BPSK bit, respectively)

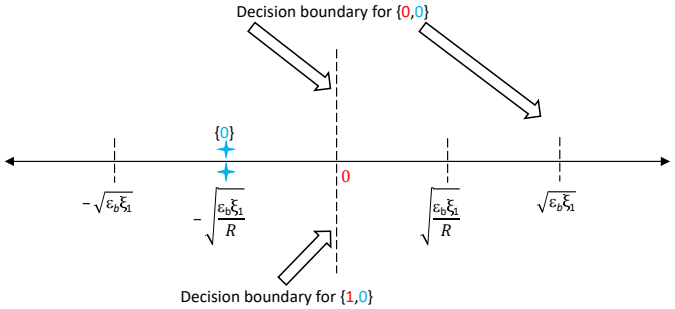

Fig. 3. Signal space diagram for u_2 with correct u_1 for (0,0) and (1,0)

different reflection coefficients to imitate similar behavior. Therefore, it is instinctive that we set the reflection coefficient for the two users as distinct as possible to aid in the NOMA process. Accordingly, ξ_1 is set as large as possible while, ξ_2 is set as small as possible. In this scenario, the signal to noise ratio (SNR) of the two users are defined as $\text{SNR}_1 = P_r\xi_1|h_1|^2/N_0$ and $\text{SNR}_2 = P_r\xi_2|h_2|^2/N_0$.

III. NOMA-BackCom BER Performance Analysis

In this section, we mathematically derive the closed-form expressions of the BER for the two BNs. Assume $2d\sqrt{\xi_1}$ $(d > 0)$ as the minimum distance between received constellation points of u_1 without AWGN. The relation between the minimum signal distance $2d$ and the bit energy ε_b can be expressed as [18]

$$d_{min} = \sqrt{\left(\log_2 M \times \sin^2\frac{\pi}{M}\right)\varepsilon_b} \quad . \tag{2}$$

For binary phase-shift keying (i.e., $M = 2$), $d = \sqrt{\varepsilon_b}$. As the signal of u_2 is superimposed on u_1 at the reader, therefore, the minimum distance between received constellation points of u_2 without AWGN is $2d\sqrt{\xi_1}/\sqrt{R}$ where R is the ratio of SNR_1 and SNR_2, i.e., $R = (\xi_1|h_1|^2)/(\xi_2|h_2|^2)$.

By virtue of its strong channel condition, u_1 is decoded first. Fig. 2 shows the constellation diagram of the composite signal received at the backscatter reader. As noted from (1), the received signal y is a superposition of two BPSK modulated information signals of two BNs, where each constellation point is represented by two bits (a_1, a_2). Here, a_1 is the BPSK bit of u_1 and a_2 is the BPSK bit of u_2. Because of the presence of IUI from u_2, a_1 is translated into two possible constellation points. The shaded block shows the two possible values that a particular u_1 bit may take due to IUI. Moreover, it is assumed that all symbols have an equal prior probability of transmission.

A. BER of the first user

For a_1, the decision boundary for bit detection is represented by the dotted line in Fig. 2 and there are four possible cases (represented by four orange stars) in which bit a_1 can be decoded incorrectly. When (0,0) is sent, the decision boundary is at a distance of $\sqrt{\varepsilon_b\xi_1} + \sqrt{\varepsilon_b\xi_1/R}$ from constellation point and if the AWGN exceeds this value, a bit error will occur due to wrong decoding of a_1. By following the same procedure for three other points, the probability that a_1 is in error is

$$P_1(e) = \frac{1}{4}\left[\text{erfc}\left(\frac{\sqrt{\varepsilon_b\xi_1} + \sqrt{(\varepsilon_b\xi_1)/R}}{\sqrt{N_0}}\right) + \text{erfc}\left(\frac{\sqrt{\varepsilon_b\xi_1} - \sqrt{(\varepsilon_b\xi_1)/R}}{\sqrt{N_0}}\right)\right], \tag{3}$$

where erfc(.) is the complementary error function.

B. BER of the second user

For decoding of u_2 bit a_2, SIC process is implemented, whereby, u_1 reconstructed bit, $\hat{a_1}$, is subtracted from received aggregate signal y. Therefore, the decoding of a_2 depends on the decoding result of a_1. This can be divided into two cases; case I: correct decoding of a_1 and case II: wrong decoding of a_1.

Fig. 3 shows the constellation diagram of a_2 when a_1 has been correctly decoded (i.e., case I). For decoding of bits {0,0} when a_1 has been correctly decoded, it can be observed from Fig. 2 that the noise must be less than $\sqrt{\varepsilon_b\xi_1} + \sqrt{(\varepsilon_b\xi_1)/R}$. Whereas, for incorrect decoding of a_2, as shown in Fig. 3, the noise must exceed $\sqrt{(\varepsilon_b\xi_1)/R}$. Therefore, the decision boundaries for a_2 in case I are $\sqrt{(\varepsilon_b\xi_1)/R}$ and $(\sqrt{\varepsilon_b\xi_1} + \sqrt{(\varepsilon_b\xi_1)/R})$. A bit error in a_2 will occur if AWGN falls within these boundaries.

For decoding {1,0}, it can be seen from Fig. 2 that AWGN should exceed $(-\sqrt{\varepsilon_b\xi_1} + \sqrt{(\varepsilon_b\xi_1)/R})$ for correct decoding of a_1. Similarly, as illustrated in Fig. 3, for incorrect a_2 decoding, AWGN should exceed $\sqrt{(\varepsilon_b\xi_1)/R}$. Therefore, the decision boundary of a_2 for decoding {0,1} in case I is $\sqrt{(\varepsilon_b\xi_1)/R}$. A bit error in decoding u_2 will occur whenever AWGN shall exceed this boundary.

In the same fashion, it can be found from Fig. 4 that the decision boundaries of a_2 decoding for {1,1} in case I are $(-\sqrt{\varepsilon_b\xi_1} - \sqrt{(\varepsilon_b\xi_1)/R})$ and $-\sqrt{(\varepsilon_b\xi_1)/R}$. Similarly, decision boundary of a_2 decoding for {0,1} is $-\sqrt{(\varepsilon_b\xi_1)/R}$ in case I as shown in Fig. 4. Therefore, the error probability of a_2 for case I can be expressed as

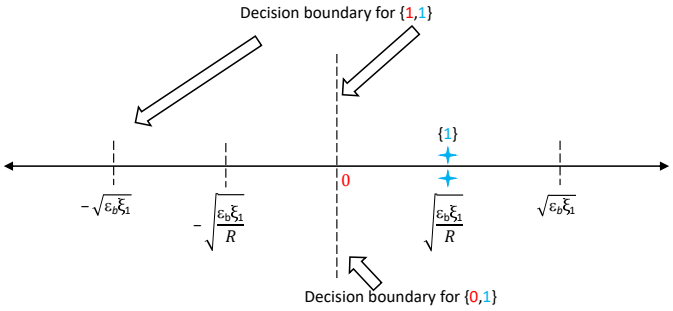

Fig. 4. Signal space diagram for u_2 with correct u_1 for (0,1) and (1,1)

$$P_{2I}(e) = \frac{1}{4}\left[2\,\mathrm{erfc}\left(\sqrt{\frac{(\varepsilon_b\xi_1)/R}{N_0}}\right) - \mathrm{erfc}\left(\frac{\sqrt{\varepsilon_b\xi_1}+\sqrt{(\varepsilon_b\xi_1)/R}}{\sqrt{N_0}}\right)\right]. \quad (4)$$

For case II, Fig. 5 describes the signal space diagram of a_2 for $\{0,0\}$ and $\{1,0\}$ scenario when u_1 has been incorrectly decoded. The decoding of u_2 will be affected by the wrong decoding of u_1 because of error propagation during the SIC process. It can be seen in Fig. 5 that for $\{0,0\}$ case, u_2 constellation point is shifted from $-\sqrt{(\varepsilon_b\xi_1)/R}$ to $(-2\sqrt{\varepsilon_b\xi_1} - \sqrt{(\varepsilon_b\xi_1)/R})$. For wrong decoding of a_1, it can be inferred from Fig. 2 that noise has to exceed $(\sqrt{\varepsilon_b\xi_1} + \sqrt{(\varepsilon_b\xi_1)/R})$. Moreover, for wrong decoding of a_2, noise has to exceed $(2\sqrt{\varepsilon_b\xi_1} + \sqrt{(\varepsilon_b\xi_1)/R})$ as shown in Fig. 5. Therefore, decision boundary for decoding a_2 for $\{0,0\}$ in case II is $(2\sqrt{\varepsilon_b\xi_1} + \sqrt{(\varepsilon_b\xi_1)/R})$.

For decoding of $\{1,0\}$ scenario in case II, it can be seen from Fig. 5 that the constellation point is shifted from $-\sqrt{(\varepsilon_b\xi_1)/R}$ to $(2\sqrt{\varepsilon_b\xi_1} - \sqrt{(\varepsilon_b\xi_1)/R})$. AWGN should be less than $(-\sqrt{\varepsilon_b\xi_1} + \sqrt{(\varepsilon_b\xi_1)/R})$ for an error in a_1 which will induce a residual error in a_2 decoding. The bit a_2 will be decoded incorrectly if AWGN is more than $(-2\sqrt{\varepsilon_b\xi_1} + \sqrt{(\varepsilon_b\xi_1)/R})$. Therefore the decision boundaries for decoding a_2 for $\{1,0\}$ scenario in case II are $(-2\sqrt{\varepsilon_b\xi_1} + \sqrt{(\varepsilon_b\xi_1)/R})$ and $(-\sqrt{\varepsilon_b\xi_1} + \sqrt{(\varepsilon_b\xi_1)/R})$.

Using the same inference technique in Fig. 6, decision boundary for incorrect decoding of user 2 BPSK bit a_2

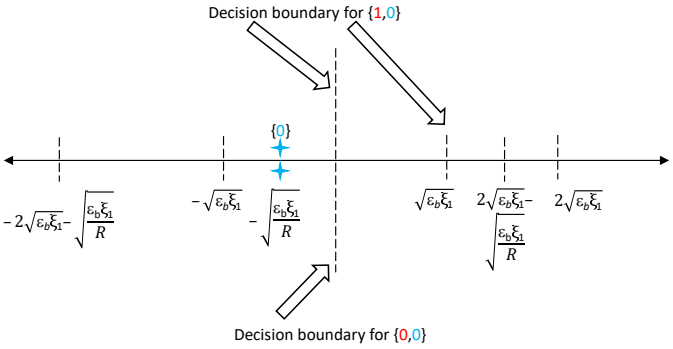

Fig. 5. Signal space diagram for u_2 with incorrect u_1 for (0,0) and (1,0)

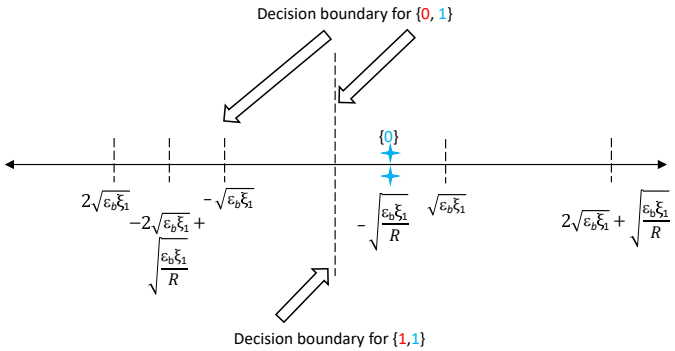

Fig. 6. Signal space diagram for u_2 with incorrect u_1 for (0,1) and (1,1)

for $\{1,1\}$ scenario in case II is $(-2\sqrt{\varepsilon_b\xi_1} - \sqrt{(\varepsilon_b\xi_1)/R})$. Similarly, decision boundaries for $\{0,1\}$ scenario are $(\sqrt{\varepsilon_b\xi_1} - \sqrt{(\varepsilon_b\xi_1)/R})$ and $(2\sqrt{\varepsilon_b\xi_1} - \sqrt{(\varepsilon_b\xi_1)/R})$ as found from Fig. 6. Therefore, the error probability of a_2 for case II can be expressed as

$$P_{2II}(e) = \frac{1}{4}\left[\mathrm{erfc}\left(\frac{2\sqrt{\varepsilon_b\xi_1}+\sqrt{(\varepsilon_b\xi_1)/R}}{\sqrt{N_0}}\right) + \mathrm{erfc}\left(\frac{\sqrt{\varepsilon_b\xi_1}-\sqrt{(\varepsilon_b\xi_1)/R}}{\sqrt{N_0}}\right) - \mathrm{erfc}\left(\frac{2\sqrt{\varepsilon_b\xi_1}-\sqrt{(\varepsilon_b\xi_1)/R}}{\sqrt{N_0}}\right)\right], \quad (5)$$

Finally, the exact average BER of u_2 over an AWGN channel can be found as the sum of two different cases given by (4) and (5) as

$$P_2(e) = \frac{1}{4}\left[2\,\mathrm{erfc}\left(\sqrt{\frac{(\varepsilon_b\xi_1)/R}{N_0}}\right) - \mathrm{erfc}\left(\frac{\sqrt{\varepsilon_b\xi_1}+\sqrt{(\varepsilon_b\xi_1)/R}}{\sqrt{N_0}}\right) + \mathrm{erfc}\left(\frac{2\sqrt{\varepsilon_b\xi_1}+\sqrt{(\varepsilon_b\xi_1)/R}}{\sqrt{N_0}}\right) + \mathrm{erfc}\left(\frac{\sqrt{\varepsilon_b\xi_1}-\sqrt{(\varepsilon_b\xi_1)/R}}{\sqrt{N_0}}\right) - \mathrm{erfc}\left(\frac{2\sqrt{\varepsilon_b\xi_1}-\sqrt{(\varepsilon_b\xi_1)/R}}{\sqrt{N_0}}\right)\right]. \quad (6)$$

IV. Numerical and Simulation Results

This section presents the numerical results in a single cluster two-user NOMA-BackCom system by evaluating the BER expressions derived in the previous section. The results are validated with Monte Carlo simulations and are found to perfectly match the derived expressions in this paper. Information symbols x_1 and x_2 for both users are selected uniformly from a BPSK constellation and passed through AWGN channels. SIC decoding is implemented at the reader, where,

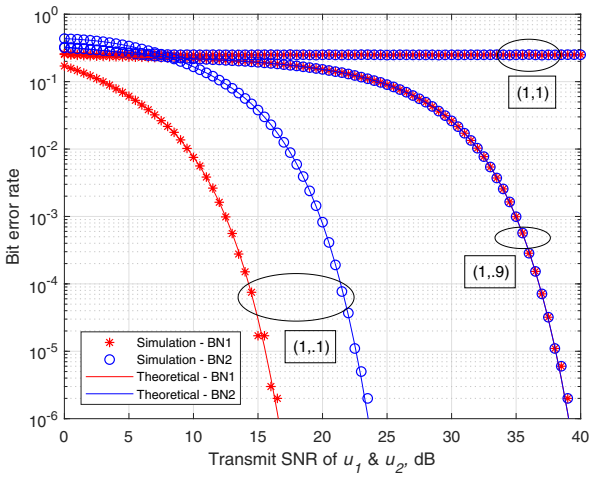

Fig. 7. BER plots of BN1 and BN2 for three reflection coefficient pairs (ξ_1,ξ_2)

u_2 is decoded after decoding and subtracting reconstructed u_1 symbols from aggregate received signal y.

In Fig. 7, numerical and simulated BER of the NOMA enhanced BackCom system is plotted against transmit SNR of both BNs. As can be seen from the figure, numerical results obtained using (3) and (6) perfectly match the simulation results for different pairs of ξ_1 and ξ_2 values. It can be observed that a greater separation in reflection coefficient values results in better BER behavior for NOMA enhanced BackCom. This is because by lowering the BN2 reflection coefficient, ξ_2, the IUI experienced by BN1 is decreased, resulting in better BER performance due to the efficient utilization of the NOMA principle. This effect is highlighted by observing the (1,1) reflection coefficient pair which is essentially a NOMA without the BackCom system and provides unacceptable performance in such a scenario.

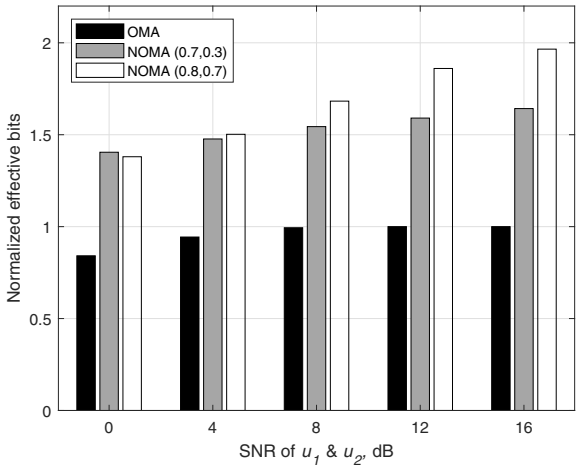

Fig. 8. Comparison of normalized effective bits transmitted in NOMA for two reflection coefficient pairs (ξ_1,ξ_2) and OMA

Fig. 8 illustrates the increase in effective non-erroneous bits transmission by employing the NOMA scheme in a BackCom system with two BNs as compared to an OMA-TDMA transmission scheme. The analysis is carried out over a sufficiently large number of time slots. It can be observed that the NOMA scheme indeed outperforms the OMA scheme due to the simultaneous transmission of two bits to the reader in a single time slot even though the OMA-TDMA scheme experiences no IUI from the second BN. Moreover, the correct transmission of bits is greatly influenced by the reflection coefficients set at the BNs. Reflection coefficients with greater separation result in better performance of the BackCom system.

In the next two simulations, analysis of reflection coefficients will be carried out to find the most optimal reflection coefficient pairs for the NOMA-BackCom system. The simulation parameters are defined in the Table. I.

TABLE I
SIMULATION PARAMETERS.

Parameters	Values
Transmit power of reader P_t	20 dBm
Noise variance N_0	-90 dBm
Path loss exponent α	2
BN1 distance from reader	25 m
BN2 distance from reader	25 m
Effective SNR of BN1 and BN2	24.08 dB

In Fig. 9, contour plot of BER is plotted by varying the two reflection coefficient pairs of BN1 and BN2. Path loss is included in both the forward and backscatter channel. The reflection coefficients of both the BNs are varied from 0.01 to a maximum value of 1 by always keeping ($\xi_1 > \xi_2$) as found from the previous result in Fig. 7. BER of BN1 is represented by a dotted line while the BER of BN2 is represented by a solid line. It can be observed from the contour plot that for any specific value of ξ_1, there exists a small range of ξ_2

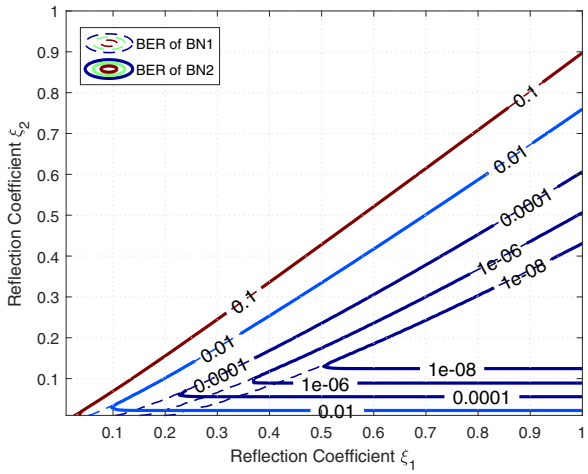

Fig. 9. BER contour plot by varying ξ_1 and ξ_2 values

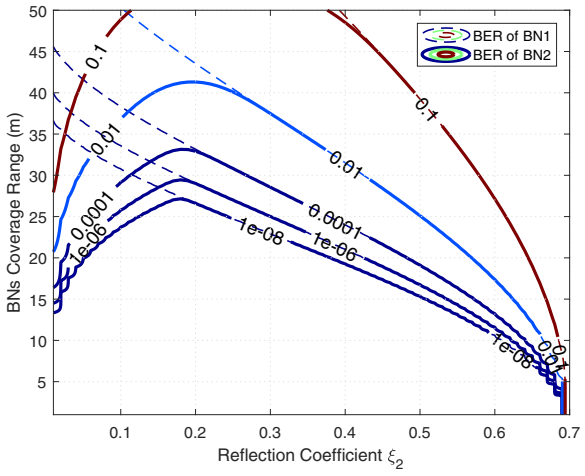

Fig. 10. BER contour plot of BackCom coverage range versus ξ_2

values smaller than ξ_1 for which we can achieve acceptable performance in a NOMA-BackCom system. This is because by increasing ξ_2, there is an increase in error propagation from BN1 to BN2 which degrades the BER performance. An interesting result of this analysis is that there is a limit for the maximum disparity between ξ_1 and ξ_2 values because if ξ_2 value is set too low, the BN2 will not be able to decode itself even with no error propagation from BN1. It should be noted that the BER performance of BN1 is independent of the value of ξ_2.

In Fig. 10, analysis of coverage range of the reader is carried out for different values of ξ_2 by setting the reflection coefficient of BN1 (ξ_1) as 0.7. It can be inferred from the figure that for the aforementioned condition, the best coverage is achieved by using ξ_2 which is almost quarter the value of ξ_1, e.g., if the Quality of Service (QoS) requirement of BER for both BN1 and BN2 is 10^{-3}, and the required coverage range for BackCom operation is 33 meters, then the reflection coefficient of BN2 could be set as 0.19 to meet these objectives. The reader's performance starts to fall off by either increase or decrease from this optimum value. Similarly, optimal values of reflection coefficients for other scenarios may be found.

V. Conclusion

This work has presented the performance of a NOMA enhanced BackCom system with imperfect SIC in terms of BER where exact closed-form BER expressions of BPSK constellation are derived for two BNs scenario over an AWGN channel. The numerical results are found to match perfectly with Monte Carlo simulations. Moreover, derived BER expressions have been evaluated for different reflection coefficients and ranges to find optimum values for each scenario. As future work, the same approach may be used for finding BER expressions for QPSK or with a higher number of BNs in a fading environment.

References

[1] Z. Dawy, W. Saad, A. Ghosh, J. G. Andrews, and E. Yaacoub, "Toward massive machine type cellular communications," *IEEE Wireless Commun.*, vol. 24, no. 1, pp. 120–128, Feb. 2017.

[2] F. Jejdling, *Ericsson Mobility Report*, Nov. 2019. [Online]. Available: https://www.ericsson.com/4acd7e/assets/local/mobility-report/documents/2019/emr-november-2019.pdf

[3] L. D. Xu, W. He, and S. Li, "Internet of things in industries: A survey," *IEEE Trans. Ind. Informat.*, vol. 10, no. 4, pp. 2233–2243, Nov. 2014.

[4] E. Sisinni, A. Saifullah, S. Han, U. Jennehag, and M. Gidlund, "Industrial internet of things: Challenges, opportunities, and directions," vol. 14, pp. 4724–4734, 2018.

[5] D. Niyato, D. I. Kim, M. Maso, and Z. Han, "Wireless powered communication networks: Research directions and technological approaches," *IEEE Wireless Commun.*, vol. 24, no. 6, pp. 88–97, Dec. 2017.

[6] N. V. Huynh, D. T. Hoang, X. Lu, D. Niyato, P. Wang, and D. I. Kim, "Ambient backscatter communications: A contemporary survey," *IEEE Commun. Surveys Tuts.*, vol. 20, no. 4, pp. 2889–2922, 2018.

[7] X. Lu, D. Niyato, H. Jiang, D. I. Kim, Y. Xiao, and Z. Han, "Ambient backscatter assisted wireless powered communications," *IEEE Wireless Commun.*, vol. 25, no. 2, pp. 170–177, Apr. 2018.

[8] W. Liu, K. Huang, X. Zhou, and S. Durrani, "Next generation backscatter communication: systems, techniques, and applications," *EURASIP J Wirel Comm*, vol. 2019, no. 1, p. 69, Mar. 2019.

[9] Z. Ding, X. Lei, G. K. Karagiannidis, R. Schober, J. Yuan, and V. K. Bhargava, "A survey on non-orthogonal multiple access for 5g networks: Research challenges and future trends," *IEEE J. Sel. Areas Commun.*, vol. 35, no. 10, pp. 2181–2195, Oct. 2017.

[10] A. Y. Kiani, S. A. Hassan, B. Su, H. Pervaiz, and Q. Ni, "Minimizing the transaction time difference for noma-based mobile edge computing," *IEEE Commun. Lett.*, vol. 24, no. 4, pp. 853–857, 2020.

[11] M. N. Jamal, S. A. Hassan, D. N. K. Jayakody, and J. J. P. C. Rodrigues, "Efficient nonorthogonal multiple access: Cooperative use of distributed space-time block coding," *IEEE Veh. Technol. Mag.*, vol. 13, no. 4, pp. 70–77, 2018.

[12] S. Qureshi, S. A. Hassan, and D. N. K. Jayakody, "Divide-and-allocate: An uplink successive bandwidth division noma system," *Transactions on Emerging Telecommunications Technologies*, vol. 29, no. 1, p. e3216, 2018.

[13] J. Guo, X. Zhou, S. Durrani, and H. Yanikomeroglu, "Design of non-orthogonal multiple access enhanced backscatter communication," *IEEE Trans. Wireless Commun.*, vol. 17, no. 10, pp. 6837–6852, Oct. 2018.

[14] S. Zeb, Q. Abbas, S. A. Hassan, A. Mahmood, R. Mumtaz, S. M. H. Zaidi, S. A. R. Zaidi, and M. Gidlund, "NOMA enhanced backscatter communication for green IoT networks," in *2019 16th International Symposium on Wireless Communication Systems (ISWCS)*. S.l: IEEE, Aug. 2019, pp. 640–644.

[15] G. Yang, X. Xu, and Y.-C. Liang, "Resource allocation in noma-enhanced backscatter communication networks for wireless powered iot," *IEEE Wireless Commun. Lett.*, 2019.

[16] Y. Liao, G. Yang, and Y.-C. Liang, "Resource allocation in noma-enhanced full-duplex symbiotic radio networks," *IEEE Access*, vol. 8, pp. 22 709–22 720, 2020.

[17] Q. Zhang, L. Zhang, Y.-C. Liang, and P.-Y. Kam, "Backscatter-noma: A symbiotic system of cellular and internet-of-things networks," *IEEE Access*, vol. 7, pp. 20 000–20 013, 2019.

[18] J. Proakis and M. Salehi, *Digital Communications, 5th edition*. McGraw-Hill Higher Education, 2007.